

NUMERICAL ANALYSIS OF SUPERCONDUCTOR RING AND SLAB IN RESPECT OF RIPPLE REDUCTION IN TOKAMAK

Toan NGUYEN

Department of Electromagnetic Theory
Technical University of Budapest
H-1521 Budapest, Hungary
Email: toan_evtsz1.evt.bme.hu

Received: January 5, 1998

Abstract

In numerical analysis superconductors are treated as non-linear conductors with virtual conductivity that is to be changed so that the current density takes the critical value according to the critical state model. The algorithm proposed by Uesaka does this by decreasing the initial virtual conductivity until the current density reaches the critical value. However, this algorithm cannot handle correctly the situation when the electric field approaches zero, which is the case when the external field becomes constant. The virtual conductivity should be increased to infinity in order to sustain the critical current. To simulate this critical state, the steady state of finite elements was introduced. Two algorithms that apply this steady state were developed, and together with the Uesaka algorithm they were used to study the application of superconductor rings and slabs to reduce magnetic ripple in the tokamak.

Keywords: numerical analysis of superconductors, ripple reduction.

1. Introduction

The finite element formulation for the numerical analysis of superconductors can be developed from the $A - \varphi$ method [1,2]. The two governing equations, one for the superconducting region and one for the air region, can be combined into one single equation: for 2-D problems it is

$$\nabla^2 A_{sc} = \mu_0 \sigma \cdot \left(\frac{\partial A_{sc}}{\partial t} + \frac{\partial A_{ex}}{\partial t} \right) \quad (1)$$

and for axisymmetric problems it is

$$\frac{\partial}{\partial r} \left(\frac{1}{r} \cdot \frac{\partial (r A_{sc})}{\partial r} \right) + \frac{\partial}{\partial z} \left(\frac{\partial A_{sc}}{\partial z} \right) = \mu_0 \sigma \cdot \left(\frac{\partial A_{sc}}{\partial t} + \frac{\partial A_{ex}}{\partial t} \right) \quad (2)$$

where A_{sc} is the magnetic vector potential due to the magnetic field generated by the superconducting current, A_{ex} is due to the external magnetic field and the virtual conductivity σ , which is defined later, equal to 0 for

the air region. According to the critical state model we have the following relationship for the superconducting region

$$\begin{cases} \mathbf{J} = J_c(|B|) \frac{\mathbf{E}}{|\mathbf{E}|} & \text{if } |\mathbf{E}| \neq 0, \\ \frac{\partial \mathbf{J}}{\partial t} = 0 & \text{if } |\mathbf{E}| = 0, \end{cases} \quad (3)$$

where J_c is the critical current density. The virtual conductivity can be expressed as

$$\sigma = \begin{cases} \frac{J_c}{|\mathbf{E}|} & \text{if } |\mathbf{E}| \neq 0, \\ \infty & \text{if } |\mathbf{E}| = 0. \end{cases} \quad (4)$$

The FEM formulation has the following matrix form

$$\mathbf{K} \cdot \underline{A}_{sc} + \mathbf{T} \cdot \frac{\partial \underline{A}_{sc}}{\partial t} = \underline{f}, \quad (5)$$

where \mathbf{K} is the stiffness matrix, \mathbf{T} is the matrix relating to the time dependence and \underline{f} is the force vector due to the external field. To solve equation (5) in time, a Θ parameter is introduced as follows

$$\underline{A}_{sc,k+1} = \underline{A}_{sc,k} + \Delta t \cdot \left[\Theta \cdot \underline{\dot{A}}_{sc,k+1} + (1 - \Theta) \cdot \underline{\dot{A}}_{sc,k} \right], \quad (6)$$

where k is the time step number. When Θ is equal to 0, 1, 0.5, 0.878 we have the *Euler scheme*, the *backward difference*, the *Crank-Nicolson formula* and the *Liniger algorithm*, respectively [3]. Premultiplying both sides with \mathbf{T} and taking the equation (5) in consideration we get the following formula

$$[\mathbf{T} + \Delta t \cdot \Theta \cdot \mathbf{K}] \cdot \underline{A}_{sc,k+1} = [\mathbf{T} - \Delta t \cdot (1 - \Theta) \cdot \mathbf{K}] \cdot \underline{A}_{sc,k} + \Delta t \cdot \underline{f}(t). \quad (7)$$

For every step the virtual conductivity σ is to be changed according to Eq. (4). Uesaka proposed the following algorithm [4] to carry out the numerical realisation of Eq. (4):

1. The initial σ of all the finite elements is set to be large enough (e.g. $\mu_0 \sigma = 10^8 \text{ S/m}^2$).
2. If the absolute value of the induced current $|\mathbf{J}| > J_c$, then σ is to be changed as

$$\sigma_{n+1} = \frac{J_c}{|\mathbf{J}|} \cdot \sigma_n$$

3. Repeat Step 2 until $|\mathbf{J}|$ of all the elements is less than or equal to the critical current density.

If we consider Eq. (4) closely, we can see that the above algorithm cannot handle correctly the situation when the electric field approaches zero, which is the case when the external field becomes constant. The virtual conductivity should be increased to infinity in order to sustain the critical current. The demonstration of this problem can be found in [2].

2. The Steady State of the Finite Elements and its Application

Let us consider the equation

$$E = \rho_f \cdot (J - J_c), \quad (8)$$

where ρ_f is the resistivity due to the viscous force acting on fluxoids. When the induced current reaches the critical value, the electric field drops to zero and as a consequence the current can flow without the energy dissipation. This equation also means that when the current reaches the critical value, it takes the steady state or it does not change. According to this meaning the steady state of a finite element of the superconducting region can be introduced as follows:

- its current is the saved (frozen) current,
- its conductivity does not need to change.

The following two algorithms are used to realise the above interpretation:

Algorithm 1

1. The initial σ of all the finite elements is set to be great enough, e.g. $\mu_0\sigma = 10^8 \text{s/m}^2$;
2. Compute the element stiffness matrices for all the finite elements;
3. Compute the element matrices and vectors for all the finite elements;
4. Assemble the element matrices and vectors into the global equation;
5. Test the state of all the elements. If they are all in the steady state, go to Step 9;
6. Solve Eq. (7) and compute the current density \mathbf{J} ;
7. If the absolute value of the induced current $|\mathbf{J}| > J_c$, then σ is to be changed as

$$\sigma_{n+1} = \frac{J_c}{|\mathbf{J}|} \cdot \sigma_n.$$
8. Repeat Steps 3–7 until the current density of all the finite elements is less than or equal to the critical current density;
9. Those elements whose current density is close to (or differs by 1%, from) the critical density are set to be in the steady state;
10. The end.

Algorithm 2

1. The initial σ of all the finite elements is set to be great enough, e.g. $\mu_0\sigma = 10^8 \text{s/m}^2$;
2. Compute the element stiffness matrices for all the finite elements;
3. Compute the element matrices and vectors; the element vectors of the steady state elements are not computed;

4. Assemble the element matrices and vectors into the global equation;
5. Test the state of all the elements. If they are all in the steady state, go to Step 9;
6. Solve Eq. (7) and compute the current density \mathbf{J} ;
7. If the absolute value of the induced current $|\mathbf{J}| > J_c$, then σ is to be changed as

$$\sigma_{n+1} = \frac{J_c}{|\mathbf{J}|} \cdot \sigma_n.$$

8. Repeat Steps 3-7 until the current density of all the finite elements is less than or equal to the critical current density;
9. Those elements whose current density is close to (or differs by 1%, from) the critical density are set to be in the steady state;
10. The end.

Step 5 is carried out in order to see if all the finite elements of the superconducting region are in the steady state. If it is the case, then the magnetic vector potential is not to be changed. The difference of the two algorithms is found at Step 3. Algorithm 1 takes into account the intrinsic diamagnetism, while Algorithm 2 does not. It can be said that Algorithm 1 is valid for the superconducting state whose diamagnetic property is significant, while Algorithm 2 is valid for the superconducting state whose diamagnetic property is negligible.

A study is performed for both the slab and the ring in order to compare their magnetising process during their application to the rippled field in the tokamak [5-9]. The ripple resulted from the discreteness of the magnet system of the tokamak and can cause ion losses. Even though the ripple that is about 1% does not endanger the power balance of the burning plasma, the ripple losses can result in serious localised heat load of the first wall [6]. The ripple can be reduced by magnetic inserts or saddle coils [7]. UCHIMOTO et al. proposed the use of high T_c slabs to reduce ripple that has the advantage of the greater ripple reduction in a higher magnetic field and the avoidance of the feed [8]. NGUYEN et al. proposed superconductor rings to replace superconductor slabs [9]. It was shown that the application of superconductor rings had some advantages over the application of superconductor slabs proposed by UCHIMOTO et al.: it makes the numerical analysis simpler and it provides a better ripple reduction. In this paper the numerical algorithms are applied to examine the ripple reduction of superconductor slab and ring. The numerical model can be seen in *Fig. 1*: for the slab case all the region ABCD is superconductor, while for the ring case only the region ABFE and the region symmetrical with it are superconductor. The boundary condition can also be taken as zero along OPQR. The ring has the dimension of 3 mm outer diameter, 1.5 mm inner diameter and 0.6 mm thickness, which is close to the dimension of the ring measured by GOUGH et al. [10]. Reported

measurements of magnetic hysteresis for single crystals of HTSC are given in *Table 1*. The result of the field computation for this small model can be scaled up to estimate the magnetic field of the real size model by applying the principles of similarity [11–12].

For time dependence computation the Liniger algorithm is chosen. The external field, whose direction is parallel with the axis of the superconductor, is modelled to change linearly at 4 mT/s, the time step is 0.4 s and the critical current is about 10^8 A/m^2 ($\mu_0 J_c = 10^2 \text{ Vs/m}^3$).

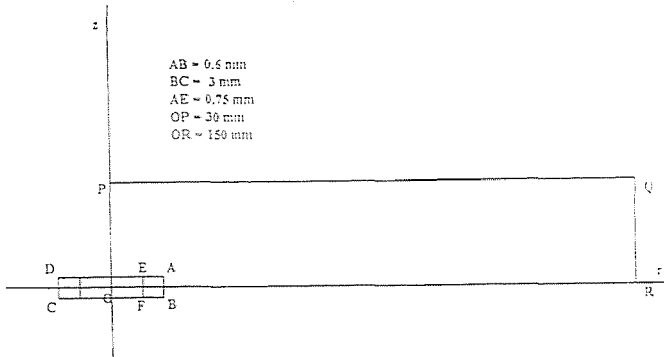


Fig. 1. The model for numerical computations

Table 1. Report of measurements of single crystals of HTSC by GOUGH et al.

Applied field	Superconductor disc	Superconductor ring
40 mT	very little flux penetrates into the body of the disc	flux starts to enter the central hole, but is still excluded from the bulk of the ring-shaped crystal
0.1 T	very little flux penetrates into the body of the disc	flux continues to enter the central hole, but very little flux penetrates into the body of the ring
1 T	little flux penetrates into the body of the disc	flux continues to enter the central hole, but still little flux penetrates into the body of the ring

Algorithm 1 is applied first. The direction of the flux penetration is similar for both the ring and the slab: that is from the outside to inside; the induced magnetic field B_z gets decreased as it goes deep into the ring or the slab. However, the minimum value of B_z can be found at the centre for the slab and near the inner edge for the ring (*Figs. 2-10*). In the case of the slab the induced magnetic field B_z increases from the field distribution of 0.005 T at the edge and -0.016 T inside at Step 10 to the field distribution of 0.01 T at the edge and -0.05 T inside at Step 40. In the case of the ring the induced magnetic field B_z increases from the field distribution of 0.005 T at the outer edge and -0.016 T at the inner edge at Step 10 to the field distribution of 0.01 T at the outer edge and -0.048 T at the inner edge at Step 40. The ring gets saturated at Step 40 (*Fig. 3*), while the slab gets saturated much slower. Even at Step 140 the critical current has not flowed fully inside the slab (*Fig. 11*). The result partly explains the experimental results measured by GOUGH et al. Very little flux penetrates into the slab for the field up to 30 mT (about Step 20). The induced field strength inside the slab is about the same with the external field strength (*Fig. 5*). However, when the external field is about 100 mT (at Step 65), the induced field strength at the centre of the slab is only about 70 mT (*Fig. 9*). This means that the net magnetic field strength inside the slab is about 30 mT, therefore a significant flux has already penetrated into the slab, while according to measurements almost no flux penetrates into the ring up to 100 mT. According to the computed result the saturation field of the slab is greater than 200 mT as at Step 140 the critical current has not circulated in all the volume of the slab. According to the measurements the saturation field must be greater than 1 T, hence the above numerical result still falls short of the experimental one. However, as it can be seen later the result computed by Algorithm 1 is still closer to the experimental result than the result computed by the Uesaka algorithm. According to the Uesaka algorithm the flux penetrates into the superconductor faster, therefore Algorithm 1 explains the difficulty of the flux penetration better than the Uesaka algorithm.

Both the numerical results, computed by Algorithm 1, and the experimental results agree that more flux penetrates into the ring than into the slab. Even though the strongest induced field of the ring is about that of the slab, the induced field at the centre of the ring is definitely smaller than this value. The difference can be observed even at Step 10. It means that at about 16 mT the flux already gets into the hole without penetrating the body of the ring (*Fig. 2*). According to the measurements this only happens at 40 mT. There are also other factors that influence the numerical result and have not been studied yet like the boundary conditions, the external field distribution, and even the dependence of the critical current density on the magnetic field.

Algorithm 2 is then applied. The result is similar in characteristic: that is the flux penetrates from the outside (*Figs. 12-17*). In the case of the slab the induced magnetic field B_z changes from the field distribution of 0.003 T

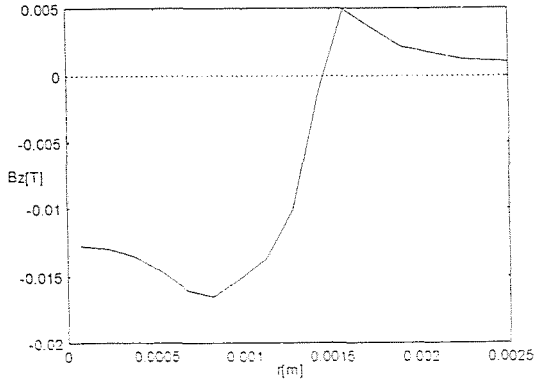


Fig. 2. Ring: the induced magnetic field B_z at step 10 (Algorithm 1)

at the edge and -0.016 T inside at Step 10 to the field distribution of 0.002 T at the edge and -0.033 T inside at Step 30. In the case of the ring the induced magnetic field B_z changes from the field distribution of 0.003 T at the outer edge and -0.016 T at the inner edge at Step 10 to the field distribution of 0.0025 T at the outer edge and -0.018 T at the inner edge at Step 30. The ring and the slab get saturated faster. The ring has the critical current flowing in all its volume at Step 15. The induced magnetic field is weaker than that given by Algorithm 1. Both Algorithm 1 and Algorithm 2 show that at low magnetic field both the ring and the slab reduce ripple similarly (Figs. 2-7, 12-15). The induced magnetic field strength near the outer edge of the ring is about the same as the induced magnetic field strength near the edge of the slab. However, Algorithm 2 shows that for higher magnetic field, when the flux penetrates deep into the slab, the field strength near the edge of the slab weakens (Figs. 16-17). Therefore according to this algorithm, the ring reduces ripple better than the slab for higher magnetic field. Algorithm 1 shows that the flux continues to penetrate into the slab against a strong magnetic shielding even when it fully penetrates the ring (Figs. 9-10). As a consequence the induced field strength near the edge of the slab continues to increase, hence for higher magnetic field the slab reduces ripple better than the ring according to this algorithm. It can be understood from these results that Algorithm 1 represents the case when the intrinsic diamagnetism plays an important role of shielding the flux from penetrating into the body of the superconductors during the magnetising process, while in Algorithm 2 the intrinsic diamagnetism is simply left out. We can say that Algorithm 1 is valid for superconductors in the Meissner state, while Algorithm 2 is valid for those in the mixed state. In the tokamak, the magnetic field is very high, therefore the mixed state is the right state of superconductors. It can be inferred from this reasoning that rings are the right ripple reducers for the tokamak.

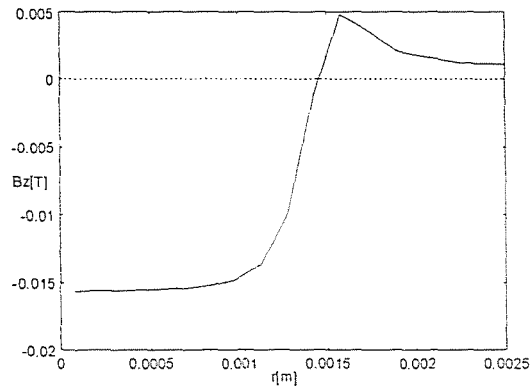


Fig. 3. Slab: the induced magnetic field B_z at step 10 (Algorithm 1)

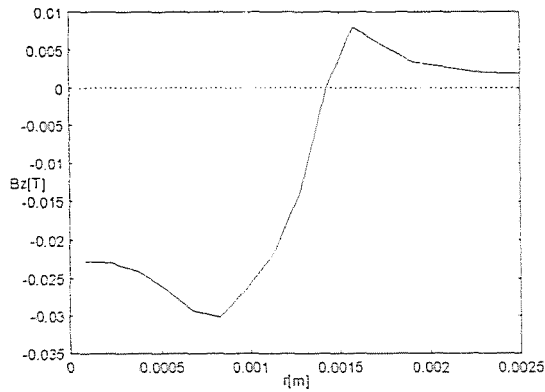


Fig. 4. Ring: the induced magnetic field B_z at step 20 (Algorithm 1)

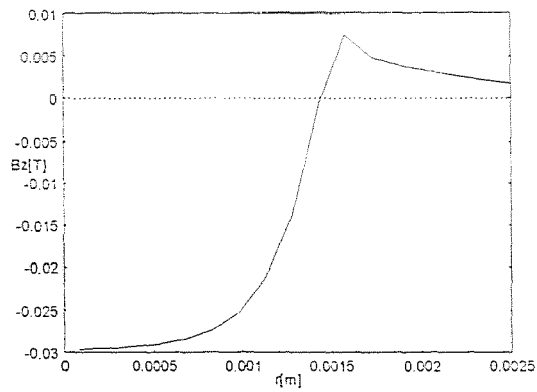


Fig. 5. Slab: the induced magnetic field B_z at step 20 (Algorithm 1)

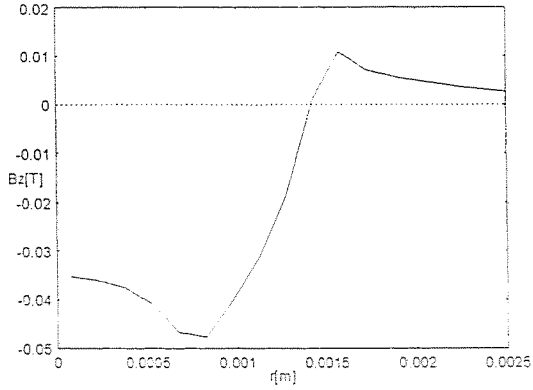


Fig. 6. Ring: the induced magnetic field B_z at step 40 (Algorithm 1)

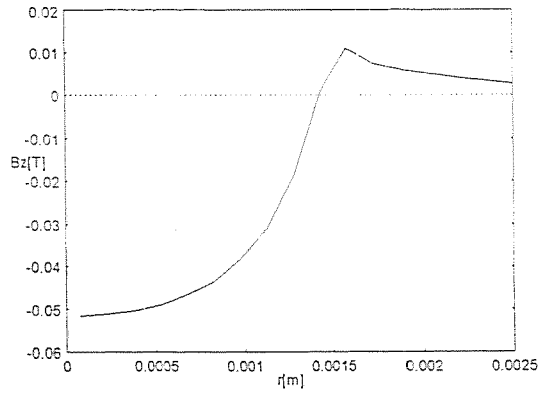


Fig. 7. Slab: the induced magnetic field B_z at step 40 (Algorithm 1)

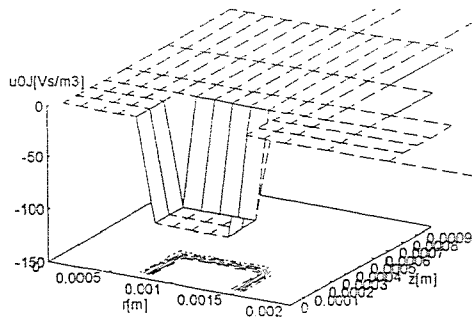


Fig. 8. The current density in the ring at Step 40 (Algorithm 1)

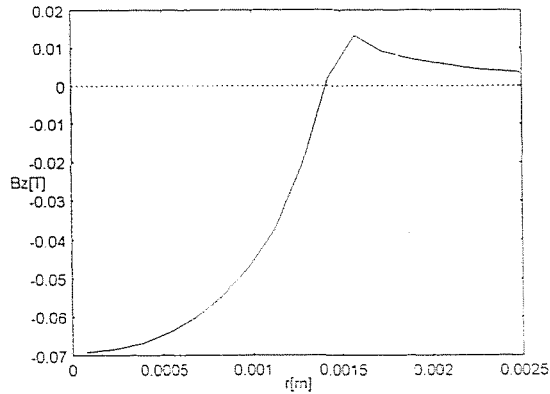


Fig. 9. Slab: the induced magnetic field B_z at step 65 (Algorithm 1)

Finally the Uesaka algorithm is also used. The trapping mechanisms are similar: that is the flux penetrates from the outside and the strongest induced magnetic field of the slab is at the centre and that of the ring is near the inner edge (Figs. 18–24). In the case of the slab the induced magnetic field B_z increases from the field distribution of 0.005 T at the edge and -0.016 T inside at Step 10 to the field distribution of 0.006 T at the edge and -0.058 T inside at Step 50. In the case of the ring the induced magnetic field B_z increases from the field distribution of 0.005 T at the outer edge and -0.016 T at the inner edge at Step 10 to the field distribution of 0.006 T at the outer edge and -0.033 T at the inner edge at Step 50. The result of the Uesaka algorithm just lies between the result of Algorithm 1 and Algorithm 2. The Uesaka algorithm takes less time for both the slab and the ring to get saturated than by Algorithm 1 and more time than Algorithm 2. The xring gets saturated at Step 25 (Fig. 22). In the Uesaka algorithm both the ring and the slab reduce ripple similarly despite the magnitude of the external field. Because the ring means less material, it would be the favoured ripple reducer.

3. Conclusion

The numerical analysis of superconductors is very difficult not only because of their non-linear properties, but also because of their dynamic and static characteristics. The attempt to treat superconductors as a kind of dynamic non-linear conductors proves to be not enough. It is quite clear from the critical state model that due to the external field change a very high supercurrent flows resistively until it drops to the critical current. After that, the critical current does not change and the steady state region can conduct without resistance. The Uesaka algorithm does not take into account the

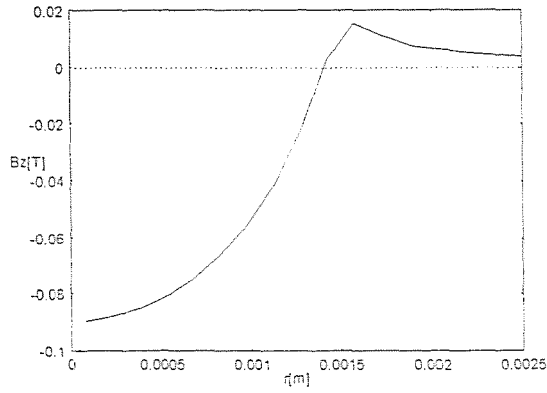


Fig. 10. Slab: the induced magnetic field B_z at step 140 (Algorithm 1)

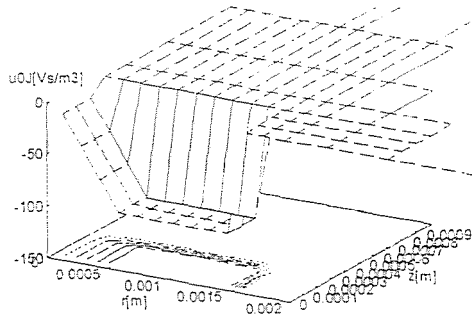


Fig. 11. Slab: the current distribution at step 140 (Algorithm 1)

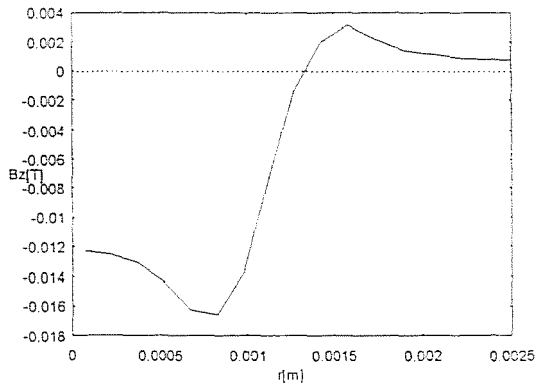


Fig. 12. Ring: the induced magnetic field B_z at step 10 (Algorithm 2)

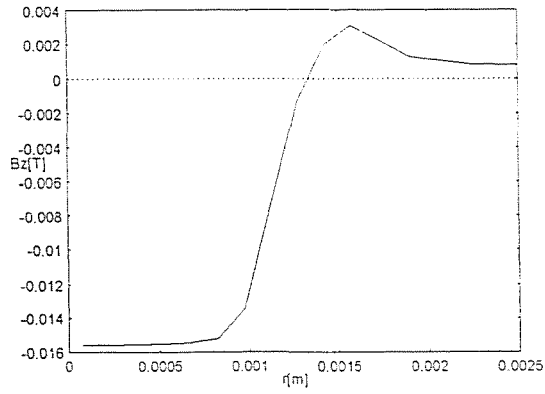


Fig. 13. Slab: the induced magnetic field B_z at step 10 (Algorithm 2)

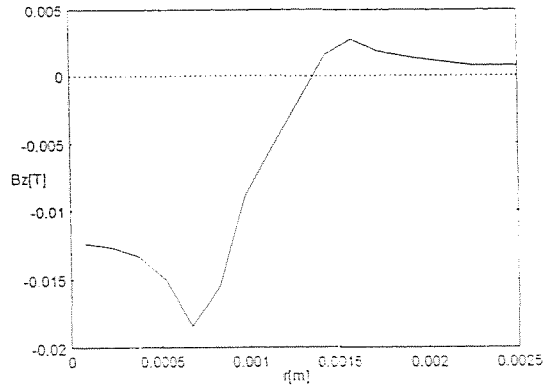


Fig. 14. Ring: the induced magnetic field B_z at step 15 (Algorithm 2)

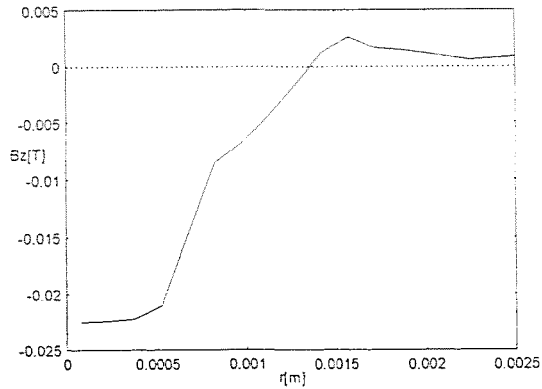


Fig. 15. Slab: the induced magnetic field B_z at step 15 (Algorithm 2)

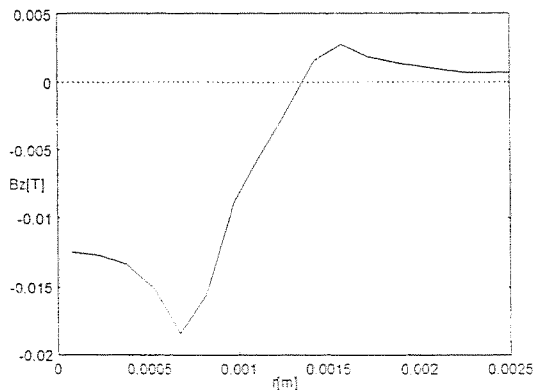


Fig. 16. Ring: the induced magnetic field B_z at step 30 (Algorithm 2)

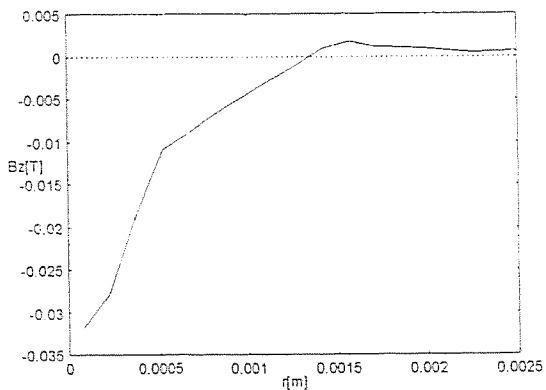


Fig. 17. Slab: the induced magnetic field B_z at step 30 (Algorithm 2)

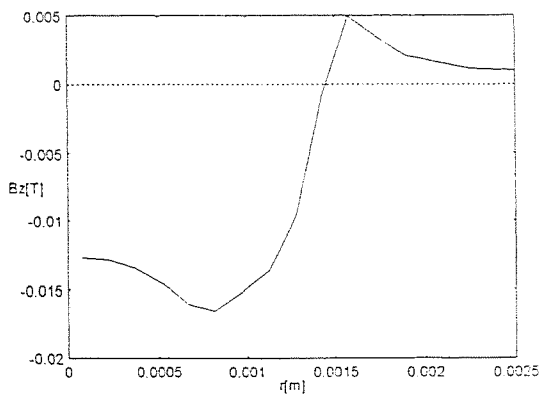


Fig. 18. Ring: the induced magnetic field B_z at step 10 (the Uesaka algorithm)

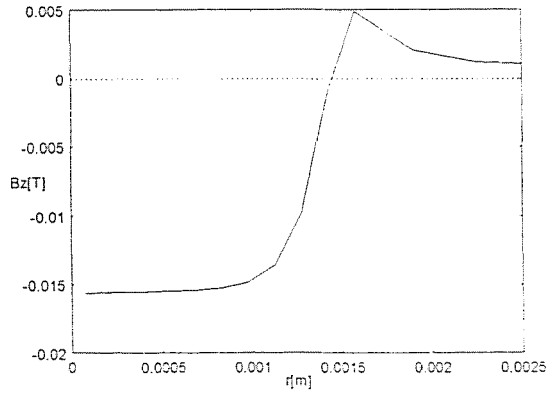


Fig. 19. Slab: the induced magnetic field B_z at step 10 (the Uesaka algorithm)

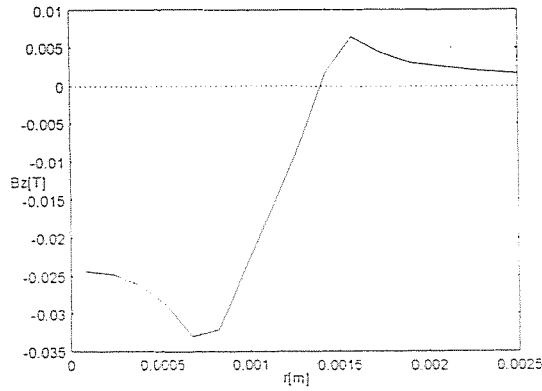


Fig. 20. Ring: the induced magnetic field B_z at step 25 (the Uesaka algorithm)

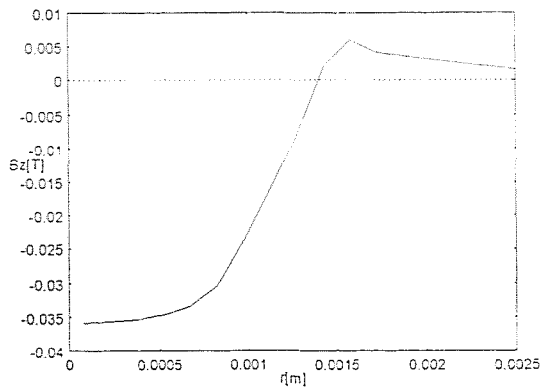


Fig. 21. Slab: the induced magnetic field B_z at step 25 (the Uesaka algorithm)

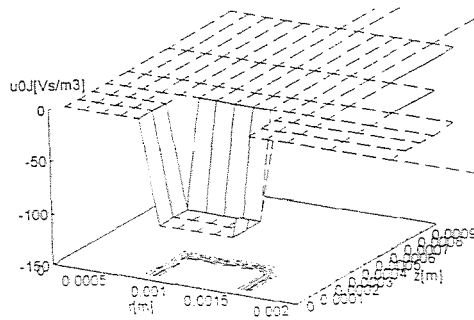


Fig. 22. The current density in the ring at Step 25 (the Uesaka algorithm)

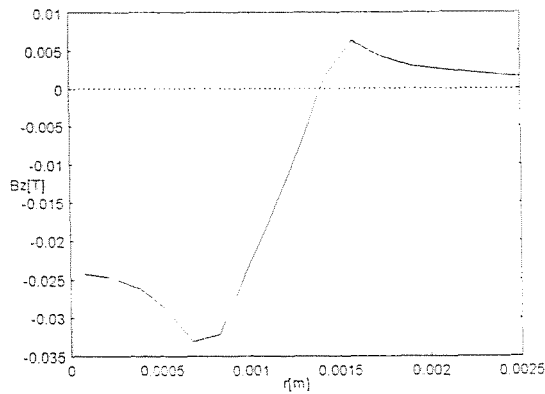


Fig. 23. Ring: the induced magnetic field B_z at step 50 (the Uesaka algorithm)

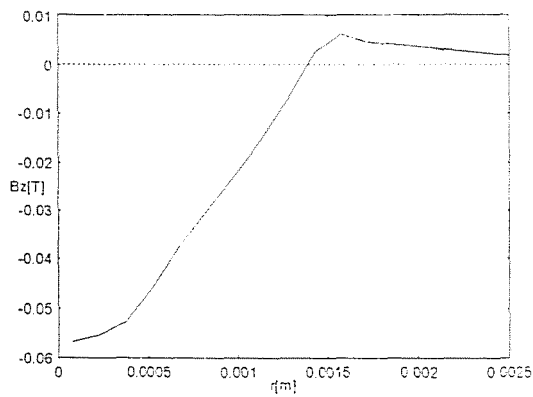


Fig. 24. Slab: the induced magnetic field B_z at step 50 (the Uesaka algorithm)

steady state and as a consequence it cannot give account for the superconducting current. The proposed algorithm is in fact an attempt to take into consideration the steady state. There is a difficulty of introducing the effect of the steady state region into the overall transient process. In the proposed algorithms the steady state is modelled as a 'superconducting' region with a frozen current. Its validity has not been confirmed experimentally. The computed result is quite short of the experimental result. However, Algorithm 1 does explain the difficulty of the flux penetrating into the slab as it takes into consideration the diamagnetic property. There are also other factors that can influence the numerical result: the boundary conditions, the external magnetic field distribution, etc. Further investigations are needed from both numerical and experimental studies.

It was shown in [9] that the ripple reduction of superconductors depends on the critical current density. At the same time, as it has been shown above the ripple reduction also depends significantly on the flux penetration into the body of the superconductors. Algorithm 1 shows that for the Meissner state little flux penetration into the body of superconductors means an increase of the field strength near the outer edge for an increasing external magnetic field. However, in the mixed state, when a lot of flux penetrates into the body of superconductors, this field weakens as it is shown by Algorithm 2. In the tokamak it is the mixed state that is dominant and in this case, rings reduce ripple better than slabs. However, further experimental investigation is needed to confirm this result.

References

- [1] SEBESTYÉN, I.: Numerical Simulation of Electromagnetic Field in Type-II Superconductors, *Periodica Polytechnica Electrical Engineering*, Vol. 38, No. 1, Technical University of Budapest, 1994
- [2] NGUYEN, T. – SEBESTYÉN, I.: Numerical Analysis for the Application of Superconductor Rings to Reduce Ripple. The 4th Japan-Hungary Joint Seminar on Appl. Electromag. in Material and Computational Technology, July, 1996. to be published in *Studies in Applied Electromagnetics and Mechanics*, edited by H. Tsuboi and I. Sebestyen
- [3] ZIENKIEWICZ, O. C. – TAYLOR, R. L.: *The Finite Element method*, Fourth Edition, McGraw-Hill 1991
- [4] UESAKA, M. et al.: Eddy Current and Force Analysis for High-Tc Superconducting Linear Drive, ISEM, Nagoya, January 1992
- [5] REDI, M. H. et al.: Collisional Stochastic Ripple Diffusion of Alpha Particles and Beam Ions on TFTR, *Nuclear Fusion*, Vol. 35, No. 10, 1995
- [6] TOBITA, K. et al.: Fast Ion Losses due to Toroidal Ripple in JT-60U, *Nuclear Fusion*, Vol. 34, No. 8, 1994
- [7] ANE, J. M.: Ripple Reduction with Magnetic Inserts and Saddle Coils, *Fusion Technology* 1994, pp. 723-726

- [8] UCHIMOTO, T. et al.: Reduction of Toroidal Ripple by Using High-Tc Superconductors, The 3rd Int. Symp. on Fusion Nuclear Technology, Los Angeles, July 1994.
- [9] NGUYEN, T. et al.: Application of Superconductor Rings to Reduce Toroidal Ripple, ISEM Cardiff, Sept. 1995
- [10] GOUGH, C. E. et al.: Transport Critical Currents, Flux Dynamics and A.C. Magnetisation of $\text{YBa}_2\text{Cu}_3\text{O}_7 - \Omega$ and $\text{Bi}_2\text{Sr}_2\text{CaCu}_2\text{O}_8$ Single Crystal Rings. Cryogenics Vol. 33, No. 3, pp. 339-346 1993.
- [11] McCAIG, M.: Permanent Magnets for Repulsion Systems, Electrical Review, 15 September 1961, pp. 425-428
- [12] BARENBLATT, G. I.: Similarity, Self-Similarity, and Intermediate Asymptotics, Consultants Bureau, New York, 1979